SANDIA REPORT

SAND97–1272 • UC–335
Unlimited Release
Printed January 1998

Seismic Monitoring of Roadbeds for Traffic Flow, Vehicle Characterization, and Pavement Deterioration

Gregory J. Elbring, Richard C. Ormesher, David J. Holcomb

Prepared by
Sandia National Laboratories
Albuquerque, New Mexico 87185 and Livermore, California 94550

Sandia is a multiprogram laboratory operated by Sandia Corporation, a Lockheed Martin Company, for the United States Department of Energy under Contract DE-AC04-94AL85000.

Approved for public release; further dissemination unlimited.

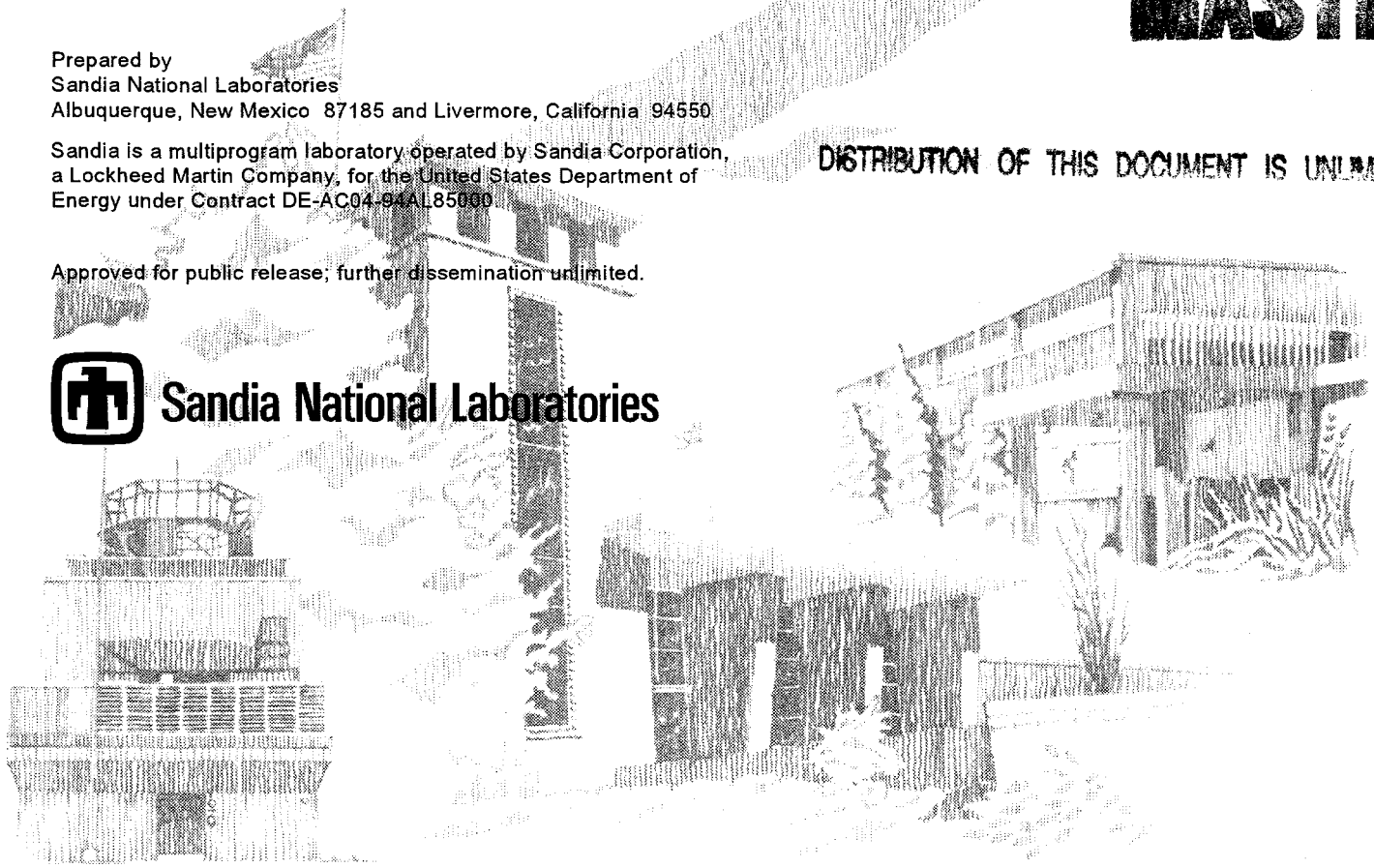

Sandia National Laboratories

DISCLAIMER

Portions of this document may be illegible electronic image products. Images are produced from the best available original document.

SAND97-1272
Unlimited Release
Printed January 1998

Distribution
Category UC-335

Seismic Monitoring of Roadbeds for Traffic Flow, Vehicle Characterization, and Pavement Deterioration

Gregory J. Elbring
Geophysical Technology Department

Richard C. Ormesher
Radar Analysis Department

David J. Holcomb
Geomechanics Department

Sandia National Laboratories
P.O. Box 5800
Albuquerque, NM 87185-0750

Abstract

A road-side seismic monitoring system has been developed that includes not only instrumentation and fielding methods, but also data analysis methods and codes. The system can be used as either a passive or active monitoring system. In the passive mode, seismic signals generated by passing vehicles are recorded. Analysis of these signals provides information on the location, speed, length, and weight of the vehicle. In the active mode, designed for monitoring pavement degradation, a vibrating magnetostrictive source is coupled to the shoulder of the road and signals generated are recorded on the opposite side of the road. Analysis of the variation in surface wave velocity at various frequencies (dispersion) is used in an attempt to develop models of the near-surface pavement velocity structure.

The monitoring system was tested at two sites in New Mexico, an older two-lane road and a newly-paved section of interstate highway. At the older site, the system was able to determine information about vehicle velocity, wheel-base length and weight. The sites showed significant differences in response and the results indicate the need for further development of the method to extract the most information possible for each site investigated.

ACKNOWLEDGMENTS

The authors wish to thank Leo Salazar of the Alliance for Transportation Research and Gordon McKean of the University of New Mexico for their invaluable help in designing and implementing the experiments, Don Schroeder for his guidance and assistance in procuring funding, and Glenn Barker and Eileen Romano for their help in the fielding aspects. This work was supported by the United States Department of Transportation, Federal Highway Administration and New Mexico State Highway and Transportation Department as well as the Department of Energy under Contract DE-AC04-94AL85000.

TABLE OF CONTENTS

ACKNOWLEDGMENTS 2

INTRODUCTION 5

DATA COLLECTION 5

INSTRUMENTATION 5
Kirtland Air Force Base Field Site *6*
Rincon Field Site *9*

DATA ANALYSIS 12

KAFB PASSIVE SEISMIC ARRAY 12
Determination of Vehicle Location *13*
Determination of Vehicle Velocity *16*
Determination of Vehicle Characteristics *16*
ANALYSIS OF RINCON FIELD SITE DATA 20
Passive Experiment *20*
Active Experiment *28*

FUTURE DIRECTIONS 31

CONCLUSIONS 32

REFERENCES 32

LIST OF FIGURES

FIGURE 1: MAGNETOSTRICTIVE VIBRATOR USED TO PRODUCE HIGH-FREQUENCY SEISMIC WAVES. 7

FIGURE 2: LAYOUT OF KAFB EXPERIMENT SITE. 8

FIGURE 3: PLAN VIEW OF RINCON TEST SITE 10

FIGURE 4: THREE-COMPONENT ACCELEROMETER CONFIGURATION ATTACHED TO MOUNTING PLATE. 11

FIGURE 5: VERTICAL-COMPONENT GEOPHONE MOUNTED TO PLATE 11

FIGURE 6: RAW DATA FROM KAFB TEST SITE RECORDED FOR A UTILITY TRUCK 13

FIGURE 7: AGC AMPLITUDE NORMALIZED PORTION OF THE DATA SHOWN IN FIGURE 6 14

FIGURE 8: AMPLITUDE MAP OF ENERGY CONTENT OF TRACES A TWO SPECIFIC TIME SLICES. 17

FIGURE 9: PLOT OF POSITION OF VEHICLE DETERMINED FROM AMPLITUDE MAP AS A FUNCTION OF TIME 18

FIGURE 10: AMPLITUDE MAP DEMONSTRATING SPLITTING OF THE PEAK. 19

FIGURE 11: COMPARISON OF WAVE AMPLITUDES GENERATED BY DIFFERENT WEIGHT VEHICLES. 21

FIGURE 12: COMPARISON OF OVERALL SIGNAL AMPLITUDE FOR VARIOUS VEHICLES, SPEEDS, AND SENSORS 22

FIGURE 13: COMPARISON OF OVERALL TRACE AMPLITUDE AS A FUNCTION OF VEHICLE WEIGHT. 22

FIGURE 14: EXAMPLE OF PASSIVE DATA RECORDED DURING THE FIRST FIELDING AT RINCON 24

FIGURE 15: EXAMPLE OF DATA TAKEN DURING SECOND FIELDING AT RINCON. 25

FIGURE 16: EXAMPLE OF DATA TAKEN DURING SECOND FIELDING AT RINCON WITH CABLES STRETCHED ACROSS THE ROAD. 26

FIGURE 17: EXAMPLE OF DATA WITH MULTIPLE VEHICLES PRESENT IN ARRAY. 27

FIGURE 18: PROCESSED DATA FROM MONOFREQUENCY BURSTS DURING FIRST RINCON FIELDING 28

FIGURE 19: PROCESSED DATA FROM MONOFREQUENCY BURSTS DURING SECOND RINCON FIELDING 29

FIGURE 20: SHEAR WAVE VELOCITY MODELS USED FOR TESTING SENSITIVITY OF SURFACE WAVE DISPERSION ANALYSIS 30

FIGURE 21: SURFACE WAVE DISPERSION CURVES GENERATED FROM VELOCITY MODELS IN FIGURE 20. 31

LIST OF TABLES

TABLE 1: SPECIFICATIONS OF SENSORS USED IN SEISMIC RECORDING 6

TABLE 2: VEHICLES USED IN KAFB TEST. 9

TABLE 3: COMPARISON OF MEASURED AND CALCULATED VEHICLE VELOCITIES. 16

TABLE 4: COMPARISON OF WHEEL BASE LENGTH WITH STANDARD DEVIATION IN VEHICLE POSITION. 19

INTRODUCTION

One of the areas of interest being investigated by the Long-Term Pavement Performance (LTPP) Division, Federal Highway Administration, is the monitoring and characterization of vehicles in motion in terms of vehicle classification and weight with an emphasis on lower cost and minimal intrusiveness. Additionally, there is an effort to investigate methods to track pavement performance. To address these interests, methods need to be developed to monitor traffic flow, determine vehicle characteristics, such as weight and dimensions, and monitor the degradation and deterioration of the pavement over time. Instrumentation for such methods must be unobtrusive and readily protected from vandalism and theft. We have begun to investigate the use of seismic sensors, both accelerometers and geophones (velocity transducers), to address these monitoring and measurement needs.

The seismic sensors are used in two different modes, depending on the need being addressed. For monitoring traffic flow and determining vehicle characteristics, the sensors are used in a passive mode, set up in an array along the edges of the roadway. The array is triggered and recorded when a vehicle enters the instrumented section of road, and the vibration and seismic waves generated by the vehicle itself are measured. Analysis of these seismic waves, both in terms of arrival time at sensors and amplitude of the waves, can be used to determine vehicle position as a function of time, vehicle velocity, and vehicle size and weight.

In the second mode of use, the sensors are again installed along the edges of the roadway. In this case, however, a controlled seismic source is activated at known locations and the seismic energy generated is recorded at the sensors. By examining surface waves induced by these active sources, mechanical properties and pavement structure can be determined. Although such analysis yields only a one-dimensional model, due to present model assumptions for derivation of the solution, using a large number of source and receiver locations should result in a pseudo-3D model of the pavement structure. Repeating the same experiment over a period of time will map out changes in the mechanical properties of the pavement and indicate regions where pavement failure will initiate.

For this investigation, both passive and active data sets were collected at two different test sites. The data collection was also performed at two different times at the second test site to examine the capability of determining changes in pavement properties over time.

DATA COLLECTION

Instrumentation

The instrumentation used in the data collection consists of three general components: seismic sensors, seismic sources used in the active mode, and a seismic recording system. Additionally, two different types of sensors were used, accelerometers for measuring particle acceleration, and geophones for measuring particle velocity. Each of these sensors has different sensitivities and frequency ranges that must be kept in mind during the data collection and analysis.

One goal of the data collection portion of the experiment was to assess the capabilities of different seismic sensors for their use in both the active and passive seismic experiments. A total of three sensor devices, two accelerometers and one geophone, were tested. The sizes, sensitivities, and frequency bands of the three sensors are shown in Table 1. All three sensors

are compact and could be installed in the highway shoulder or median with little or no visible equipment.

Sensor	Diameter	Height	Sensitivity	Low Freq.	High Freq.
Wilcoxon 731-20 accel.	1.00 inches	1.1 inches	20 V/g	1 Hz	1300 Hz
Wilcoxon 726 accel.	0.54 inches	1.4 inches	100 mV/g	3 Hz	15000 Hz
Mark Products L-28 geophone	1.25 inches	1.4 inches	2.02 mV•s/in	4.5 Hz	300 Hz

Table 1: Specifications of sensors used in seismic recording.

For the active seismic experiments, seismic sources must be used to generate energy at a given location, and, if possible, at a given frequency. Two sources were used to generate seismic energy. The first of these was a simple 20-pound sledge hammer wired with an impact trigger to initiate data recording when source impact occurs. This source produces a fairly sharp wavelet containing a range of frequencies, but dominated by lower-frequency (< 500 Hz) energy.

The second source used was a magnetostrictive actuator (Figure 1) manufactured by Etrema Products, Inc. (model 110/12 -MP). These actuators consist of a rod of magnetostrictive material surrounded by a coil. Magnetostrictive materials have the property of changing length when a magnetic field is applied and can be made to lengthen or shorten by varying the current in the coil. When an AC current is applied, the magnetostrictive actuator vibrates at the frequency of the AC current. To generate the desired source signal, the actuators are driven with the amplified output of a standard function generator and can output frequencies from 200 Hz to 2500 Hz. The control provided by the function generator allows constant monofrequency, swept frequency, or short-burst monofrequency signals to be produced.

Data were recorded on standard seismic recording instrumentation. The first set of test data were recorded using an EG&G ES2420 model seismograph with 48-channel capability and 16 bit analog-to-digital converters. For the second set of experiments, an OYO DAS-1 recording system was used that also has 48-channel capability but uses a 32-bit analog-to-digital converter allowing a greater dynamic range of values to be recorded, an important factor when dealing with the range of seismic sensor sensitivity and source amplitudes involved in this study.

Kirtland Air Force Base Field Site

An initial test of the passive system only was performed on Kirtland Air Force Base (KAFB), Albuquerque, New Mexico in July of 1995. A section of north-south two-lane road in the east-central portion of the base was instrumented with the geophones only. The section of road used was level, and the pavement was in good shape but showing signs of age. There were no noticeable flaws or significant bumps in the pavement section used. The road was straight along the instrumented section, but curved to the left just north (within 50 feet) of the end of the experiment site. Typical speeds for vehicles traveling on this section range from 35 to 60 mph.

Vertical component geophones were emplaced along both sides of the road at 20-foot spacings (Figure 2). Nine geophones were coupled to the ground with a 4-inch spike inserted into the ground on each side of the road for a total length of 160 feet. A manual trigger was used to start the recording instrument when the north-bound vehicle passed a point 34 feet south of sensors 1 and 18 (lower dot-dash line on figure). A second manual trigger was used to insert a pulse onto an unused recording channel when the vehicle passed sensors 9 and 10 and exited the

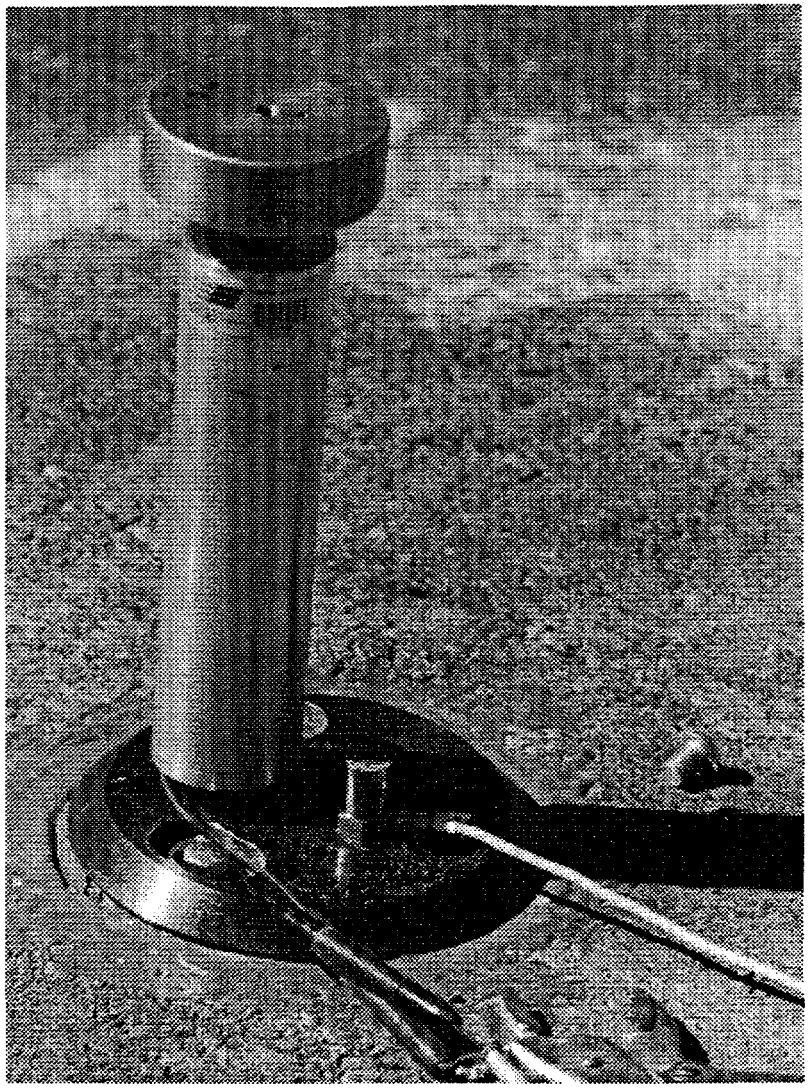

Figure 1: Magnetostrictive vibrator use to produce high-frequency seismic waves. Brass cylinder on top serves as a reaction mass. Note 6-inch diameter mounting plate bolted to pavement and accelerometer mounted to the same plate at the base of the shaker to record a source signature.

sensor array (upper dot-dash line). This gives a crude, but independent measure of the vehicle velocity.

For testing purposes, four vehicles with known characteristics were driven north-bound through the array at two speeds, 30 and 50 mph. Vehicle descriptions and weights are given in Table 2. Data recording was initiated when the vehicle passed the trigger point as discussed in the previous paragraph and recorded for a total of 8 seconds at a sampling rate of .0005 seconds (.5 ms). Data were recorded on the EG&G seismograph and stored in the field on 9-track tapes. Additional data were collected recording a sledge hammer blow on the pavement at a location 10.3 feet west of station 1.

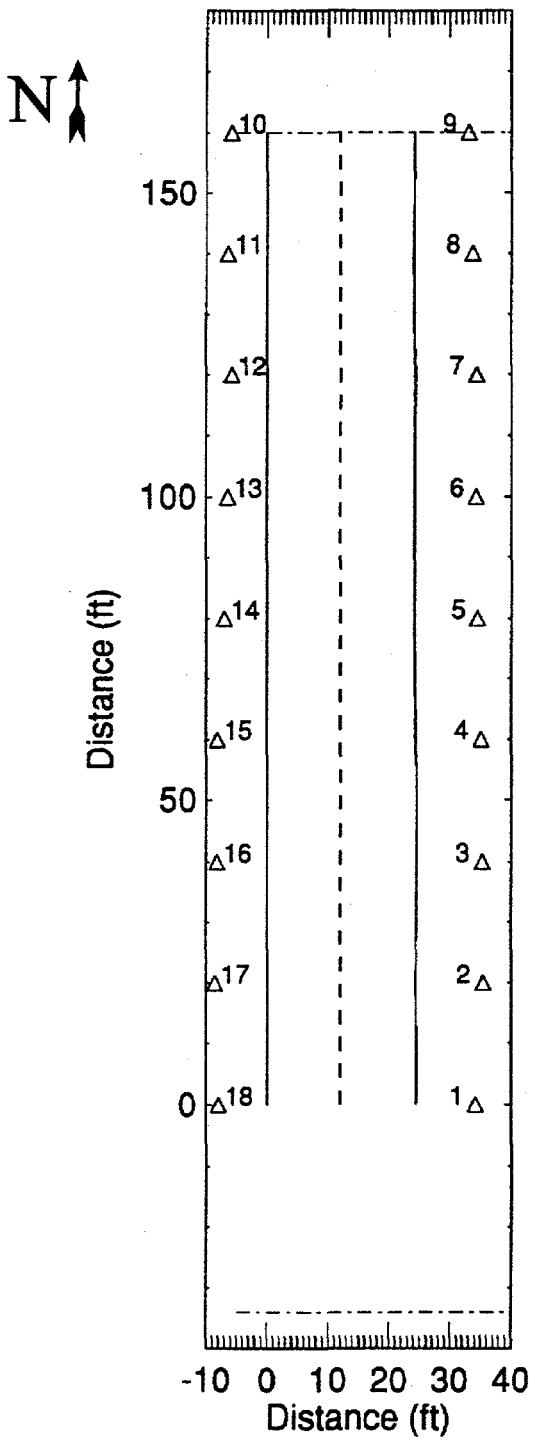

Figure 2: Layout of KAFB experiment site. Triangles represent station locations with the sensor numbers corresponding to the trace numbers in the following figures. Dashed lines represent points where manual speed measurement marks were recorded when the vehicle entered and exited the array.

Vehicle	Length	Weight
Land Rover (50 mph only)	7.3 ft.	3260 lb.
Pick-up Truck	12 ft.	5020 lb.
Utility Truck	13 ft.	10980 lb.
Flat-Bed Truck	no data	15860 lb.
Instrument Truck	24 ft.	26320 lb.

Table 2: Vehicles used in KAFB test.

Rincon Field Site

The second field site used was a section of northbound Interstate 25 located one mile north of the Rincon, New Mexico exit. The road bed at this location was constructed as part of the Strategic Highway Research Program (SHRP) and consists of 4 inches of plant-mixed bituminous pavement (PMBP) underlain by 4 inches of Type IB bituminous treated base and 4 inches of Type IB base. Both accelerometers and geophones were used at this site to determine the advantages and disadvantages of each of the three sensor types. Sensors were spaced along the shoulder and median at 30-foot intervals (see Figure 3) for a total array length of 150 feet. To mount the sensors during the initial test, holes were drilled in the shoulder pavement, and steel mounting plates were bolted to the pavement with concrete anchors. The mounting plates were pre-drilled for the mounting studs on the accelerometers (Figure 4) and for the magnetostrictive actuators (Figure 1). An additional hole was drilled adjacent to the plates to accommodate the geophone spike for geophone emplacement (Figure 5).

The first portion of the Rincon experiment, conducted in early December, 1995, used the active seismic method to attempt to define a baseline pavement structure to compare to future surveys to isolate regions of the pavement showing undesirable changes in mechanical properties. At the time of the survey, the road had been opened to traffic for less than three weeks, so that the baseline survey should show little pavement degradation.

For this active experiment, both the magnetostrictive vibrator and the sledge hammer were used to generate seismic waves. Sledge hammer blows were conducted within 3 feet of the same mounting plates used for mounting the accelerometers. The magnetostrictive vibrator was attached to these same mounting plates and run in two different modes: a burst mode where the source vibrated for 3 cycles at a monofrequency with these bursts repeated at a .05 second interval; and a swept-frequency mode sweeping linearly from 200 Hz to 2000 Hz in 2 seconds. Frequencies for the bursts also ranged from 200 Hz to 2000 Hz in 100 Hz intervals.

Three component data were collected at the median-side stations 7 through 12 and at station 1 using the Wilcoxon 731-20 accelerometers. These were the only sensors of the three types listed in Table 1 that had both the sensitivity range required and a reasonable frequency range, even though they will not perform well above 1300 Hz. For each of the median-side receivers, sledge hammer blows from each of the shoulder-side stations (1-6) were recorded for 512 ms at a sample rate of 0.125 ms. This configuration results in source-receiver separations ranging from 40 ft to 155 ft. Energy output from the vibrator was significantly less than the hammer source. For this reason, vibrator data, both bursts and sweeps, for each source location on the shoulder-side were recorded only at the three nearest receiver locations on the median side of the highway (i.e. the receiver location directly across from the source and the first receiver location on either side of this station). This results in a maximum source-receiver separation of 50 ft. Bursts were recorded for 512 ms at 0.125 ms sampling rate, and the frequency sweeps were recorded for 2048 ms at the same sampling rate.

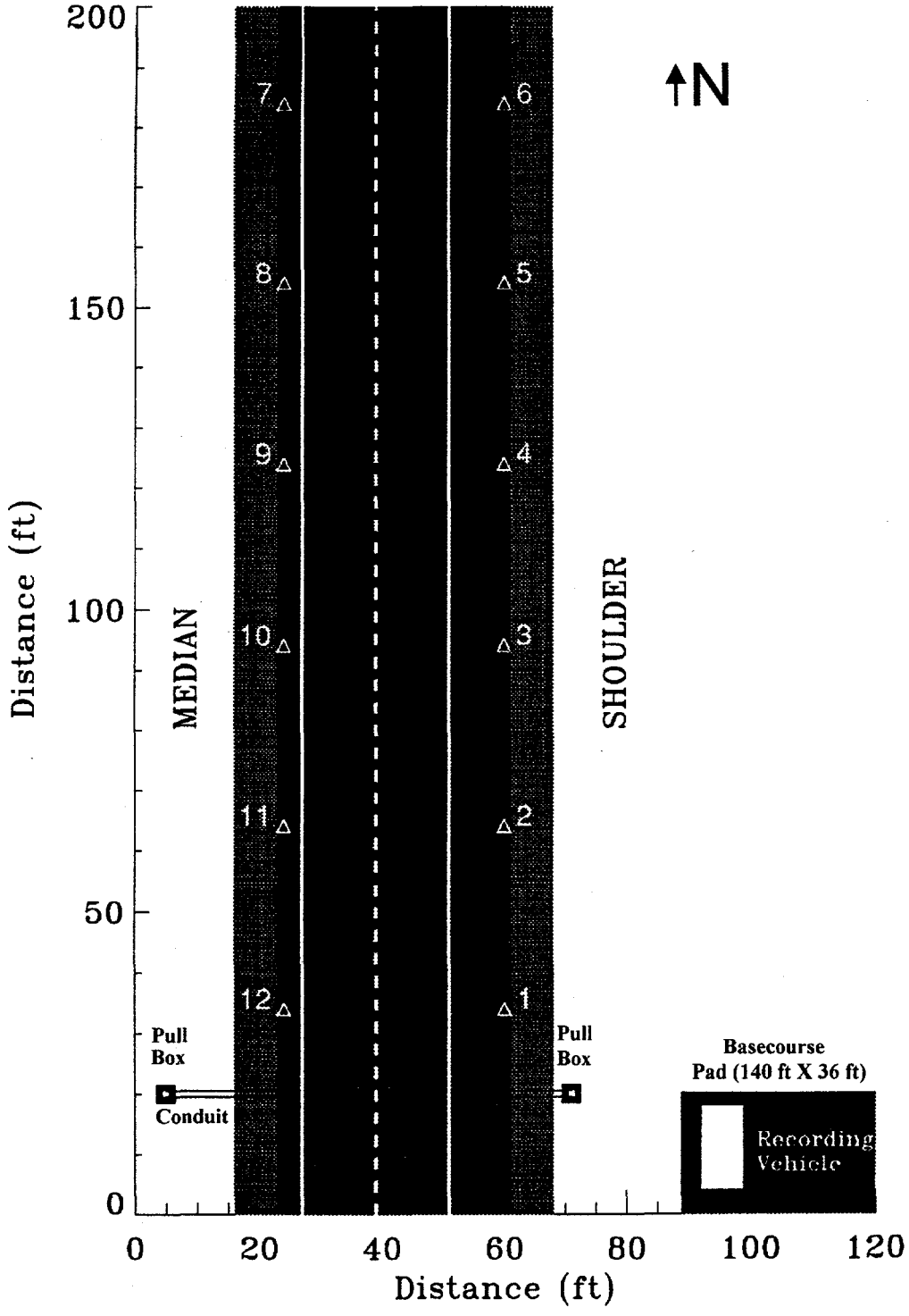

Figure 3: Plan view of Rincon test site showing north-bound lane of I-25. Triangles represent sensor and source locations. Sensors on the median side of the road were connected to the recording truck by cables passed under the highway through the conduit and pull boxes.

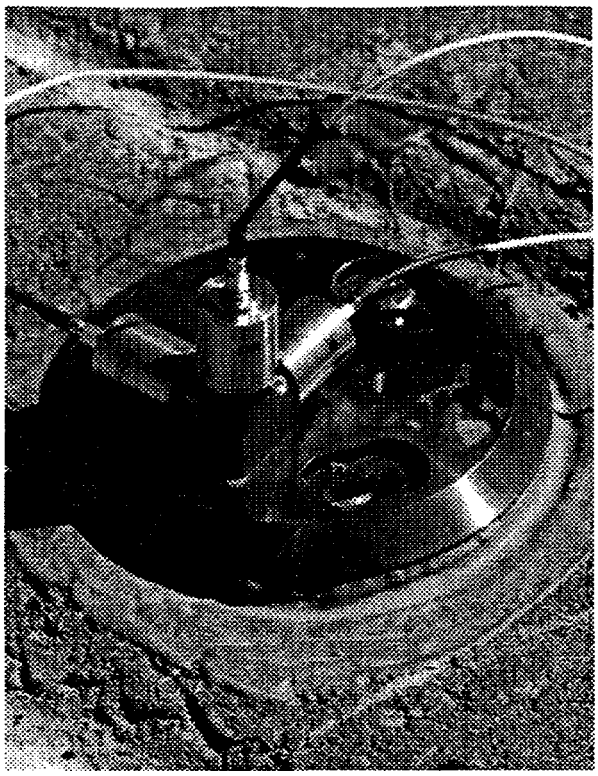

Figure 4: Three-component accelerometer configuration attached to mounting plate.

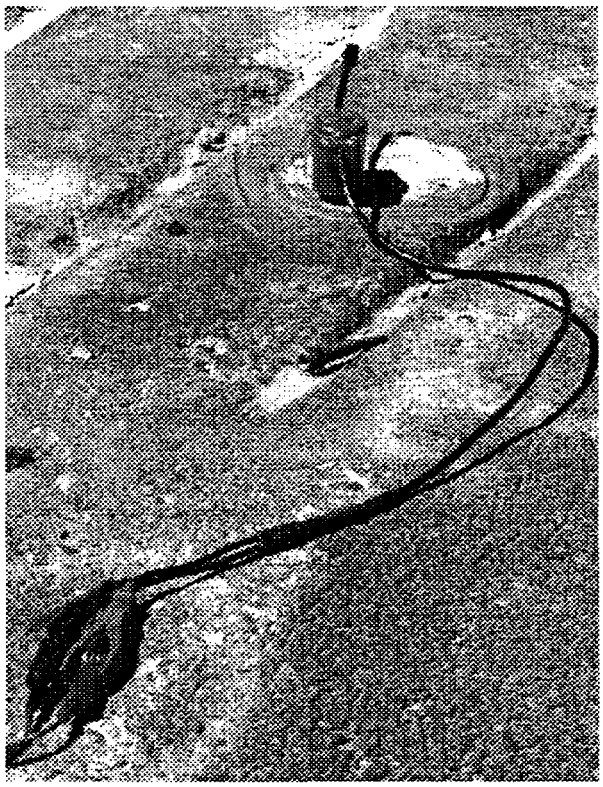

Figure 5: Vertical-component geophone mounted to plate (second Rincon fielding).

A passive seismic experiment similar to that outlined in the KAFB field site description was also performed at this site. Vertical-component geophones were emplaced at each of the station locations (1-12) shown in Figure 3. At station 1, one of each of the Wilcoxon accelerometers was also mounted on the plate to measure the vertical particle acceleration. Having data from all three sensor types will enable us to determine which of these sensors has both the most desirable sensitivity and frequency range for passive monitoring.

Data for the passive array were recorded for 4096 ms at a sampling rate of 0.25 ms. Uncontrolled traffic was recorded by manual triggering of the recording system when an interesting vehicle configuration was entering or within the limits of the array. Photographs were taken to record the vehicle configuration each time the recording system was triggered. A variety of single vehicles and multiple vehicle configurations were recorded to test the system performance in a real-world situation.

A second data set was recorded at the same site in March, 1996 to look at changes in the site over time. During the first fielding, the attachment of the mounting plates directly to the pavement was determined to be an inefficient way of coupling the seismic energy to the ground. For the second fielding, concrete plugs the same diameter as the mounting plates were cast with threaded studs protruding from the top to which the mounting plates could be bolted. Holes were bored into the shoulders of the highway that would accommodate the cement plugs, and the plugs were epoxied into these holes. This provided a much stiffer coupling of the actuators to the pavement and preserved the higher frequencies.

DATA ANALYSIS

KAFB Passive Seismic Array

Raw true-amplitude data recorded with the passive seismic array during the passage of the utility truck at 30 mph is shown in Figure 6. The vehicle enters the array between stations 1 and 18 and, as time progresses, travels between the stations on opposite sides of the road until it exits the array between stations 9 and 10. The signal amplitude at any one station increases as the vehicle approaches and decreases after the vehicle passes forming a packet of energy readily visible in the seismic section (e.g. trace 9 from 3 to 6 seconds). As the vehicle passes through the array, the energy packet occurs at different times at each sensor forming the triangular pattern from trace to trace characteristic of all the seismic sections. When the distance between adjacent sensors is taken into account, the inverse of the slope of the line formed by these energy packets gives a rough estimate of the vehicle velocity, in this case, 20.5 ft/s (30 mph).

There is another notable feature in the signals recorded. Several higher amplitude, short duration events are seen that show a coherency from trace to trace, such as the event between the arrows on Figure 6. These travel at a much more rapid velocity (about 700 ft/s) than the vehicle. This faster velocity matches quite well the velocity of seismic surface waves at the site measured from the data generated by the sledge hammer blows. The vehicles, then, are generating numerous small seismic events that are propagating through the array.

With the true trace amplitudes shown in Figure 6, it is difficult to follow the short duration events across all the traces. An amplitude normalization technique known as Automatic Gain Control (AGC) is often applied in such cases in exploration seismology. This normalization

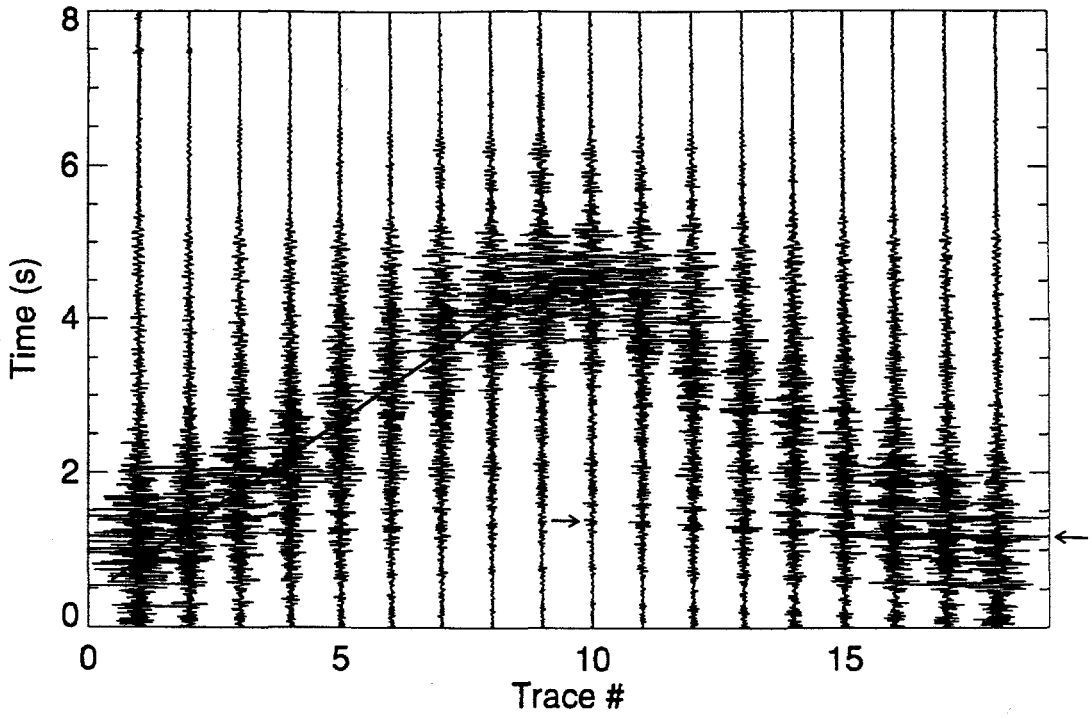

Figure 6: Raw true-amplitude data from KAFB test site recorded for a utility truck passing through the array at 30 mph.

scheme not only results in nearly constant amplitudes from trace to trace, but also normalizes the amplitudes through time in each trace.

To apply AGC, each trace was divided into fixed time windows of .5 seconds. This window length was chosen to be 10 times the period characteristic of most of the short duration event wavelets (i.e. the characteristic wavelet). A root-mean-square (RMS) amplitude value was determined within each window for each trace, and the ratio of this value to a normalized amplitude value (1.0) was assigned to the center point of each time window. The gain to apply at any sample point is then calculated by interpolating between the gains determined at the time-window centers. Figure 7 is a portion of the same data set shown in Figure 6 with AGC applied. With this gain shift in place, it can now be seen that the packets of energy are composed primarily of these small individual seismic events of varying amplitude. In addition, the general shape of these arrivals varies as a function of the location of the vehicle within the array. By examining the timing and coherency of these arrivals, the location of the vehicle can be determined.

Determination of Vehicle Location

The method developed for determining the vehicle location is based on the degree of match between predicted arrival times from any given source location and the actual data recorded. The roadway is mathematically gridded over the entire experiment area to give a range of possible locations of the vehicle. The travel time from each possible location to each recording station is calculated either absolutely or as a travel time delay between a reference station and the recording station. This calculation is a function of the separation distance involved and the

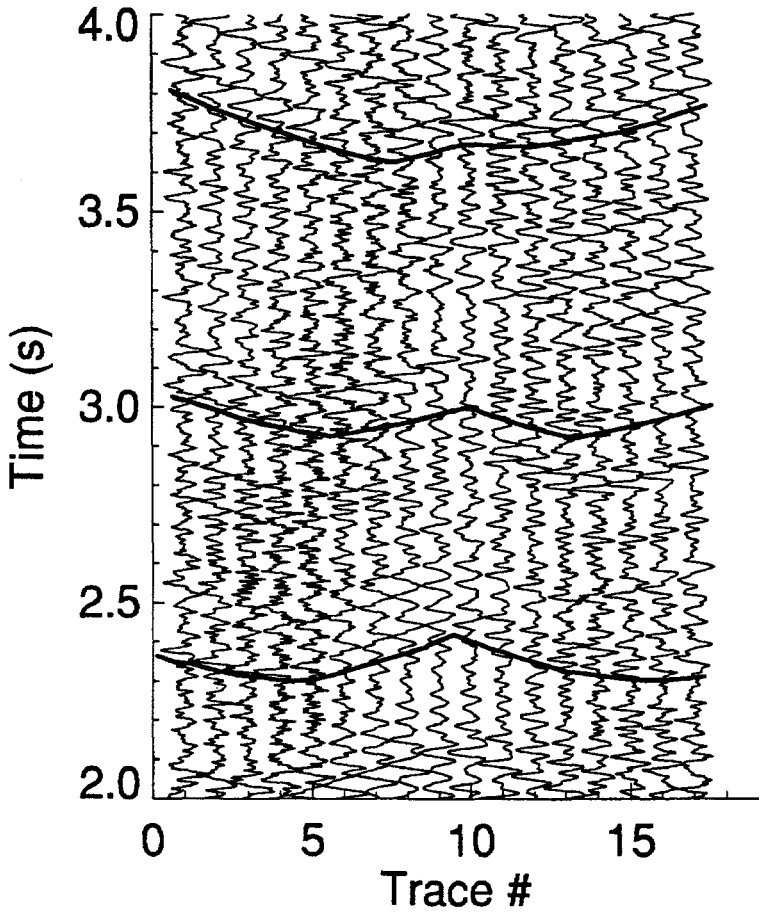

Figure 7: RMS amplitude normalized portion of the data shown in Figure 6. General shape of three selected arrivals marked with thick lines.

surface wave velocity determined from a controlled source recording (for this site, 700 ft/s). If the source location is the correct one, a coherent wavelet should be apparent on each trace at the calculated travel time.

When determining the source location using absolute travel times, the sum of the amplitude of each trace at the calculated arrival time from each grid point is generated. This sum is then weighted by the inverse of the standard deviation of the amplitudes used to create the sum. This standard deviation should be small when coherency between sensors is high. Since the wavelet generated by the vehicle has a certain time length, the individual weighted sums are then summed in time by a characteristic wavelet length, in this case .05 seconds, and this final value is assigned to the grid point. This procedure is calculated for all grid points (possible source locations).

This procedure can be described mathematically by first letting $a_m(t)$ denote the AGC-scaled time sequence of the signal sampled at the m^{th} sensor. The sensors in the array are located at positions $\{x_m , y_m\}$, m=0,...,M-1, where M is the total number of sensors in the array. The weighted sum of the amplitudes can be expressed as

$$g_{ij}(t) = \frac{\sum_{m=0}^{M-1} a_m(t + \Delta_{ijm})}{\sigma_a(t)}$$

where Δ_{ijm} is the calculated travel time from the possible source location, grid point (i, j) to receiver m and $\sigma_a(t)$ is the standard deviation of $a_m(t)$ for all sensors at time $(t + \Delta_{ijm})$. These values are further summed over the time length of the characteristic wavelet, t_w, to give the final value $G_{ij}(t)$ for the possible source point (i, j) at time t

$$G_{ij}(t) = \sum_{\tau=t}^{t+t_w} g_{ij}(\tau)$$

In a similar manner, a value for each possible source point can be found using the relative travel time between a chosen reference station and the m^{th} sensor. We define the delay and sum of the sensor outputs to be

$$z_{ij}(t) = \sum_{m=0}^{M-1} a_m(t - \Psi_{mij})$$

where $\{i, j\}$ is the coordinate index for the assumed source location $\{x_i, y_j\}$ and Ψ_{mij} is the time-delay difference between the time delay from the assumed source location to the m^{th} sensor and the time delay from the assumed source location to a reference sensor. The time delay difference, Ψ_{mij}, is calculated as follows:

$$\Psi_{mij} = c\Delta R = c\left(R - \sqrt{(x_i - x_m)^2 + (y_j - y_m)^2}\right)$$

where c is the signal propagation speed (700 ft/s), R is the radial distance from the assumed source location to a reference sensor, and $\{x_i, y_j\}$ is the assumed source location.

The total energy within the time window generated from the assumed source location is calculated by squaring and summing as follows:

$$E_{ij} = \sum_{\tau=t}^{t+t_w} z_{ij}^{\,2}(\tau)$$

where t_w is again the length of the characteristic wavelet.

The total energy values, E_{ij}, or the weighted sums, G_{ij}, for each possible source location calculated in the manner above can be contoured over the gridded region. Figure 8 shows shaded contour maps of the weighted sums generated from the data shown in Figures 6 and 7 for times of 2.421 seconds and 2.841 seconds after the initiation of recording. The bright spot in each of the plots pinpoints the best fit for the actual vehicle location. Note the vehicle motion indicated by the change in position of this bright spot. Mapping either the total energy values or the weighted sums produced very similar results.

Determination of Vehicle Velocity

Either of the location procedures outlined above can be done with as small a time step as desired down to the sampling rate of the original data. This provides vehicle position as a function of time. For each time step, the location of the peak along the road (Y-axis) can be determined and plotted versus time (Figure 9). A line can be fit through these data and the inverse slope of this line gives the average vehicle velocity for the time period analyzed. Different velocities will be expressed as different slopes for the lines fit, as can be seen by comparing Figures 9b and 9d.

At the KAFB test site, the velocities determined by the seismic analysis can be compared to the average velocity of the vehicle through the array based on the timing marks generated manually during recording. These manual timing marks have an estimated accuracy of ± .5 s giving an estimated error in velocity of ± 5 mph. Table 3 compares the velocity determined manually and through the seismic analysis for trials with complete data sets. Most of the values agree within the ± 5 mph error range.

Vehicle	Measured Velocity	Calculated Velocity
Land Rover	42 mph	43 mph
Pick-up Truck	31 mph	31 mph
Utility Truck	27 mph	31 mph
Utility Truck	47 mph	53 mph
Flat-Bed Truck	26 mph	29 mph
Flat-Bed Truck	39 mph	47 mph

Table 3: Comparison of measured and calculated vehicle velocities.

Determination of Vehicle Characteristics

Closer examination of the data collected by the passive array has yielded additional information on the characteristics of the vehicle itself, specifically vehicle length and weight. Although the correlation analysis of data features with these vehicle measurements is still in the early stages, initial results look promising.

A rough estimate of the vehicle length appears to be contained in the velocity plots discussed in the section above and seen in Figure 9. We noticed that these position-versus-time plots had different amounts of data scatter for different vehicles. This can be seen by comparing the two lines in 9a and 9b. In the contour maps, this same scatter is expressed by splitting of the peak into two bright spots (Figure 10) and is seen frequently as the analysis proceeds through the time steps. In general, the longer the vehicle's wheel base, the greater the amount of scatter in the position versus velocity plot. We theorize that this scatter results from different wheels of the vehicle generating the small seismic events at different times so that the determined vehicle position jumps back and forth between the position of the front wheels and the position of the rear wheels. The standard deviation of the vertical-axis scatter about the line fit to the position-versus-time plot gives a rough estimate of the length of the vehicle (Table 4). This estimate also appears to be velocity dependent with the standard deviation decreasing with increasing velocity. Unfortunately, we do not have enough data to derive an empirical relation to determine a more exact value of the wheel-base length from the standard deviation or to determine how axle configuration and load distribution may affect these estimates. Similar side-to-side peak splitting from left and right tires is not observed due to poor horizontal resolution as a result of the sensor array geometry.

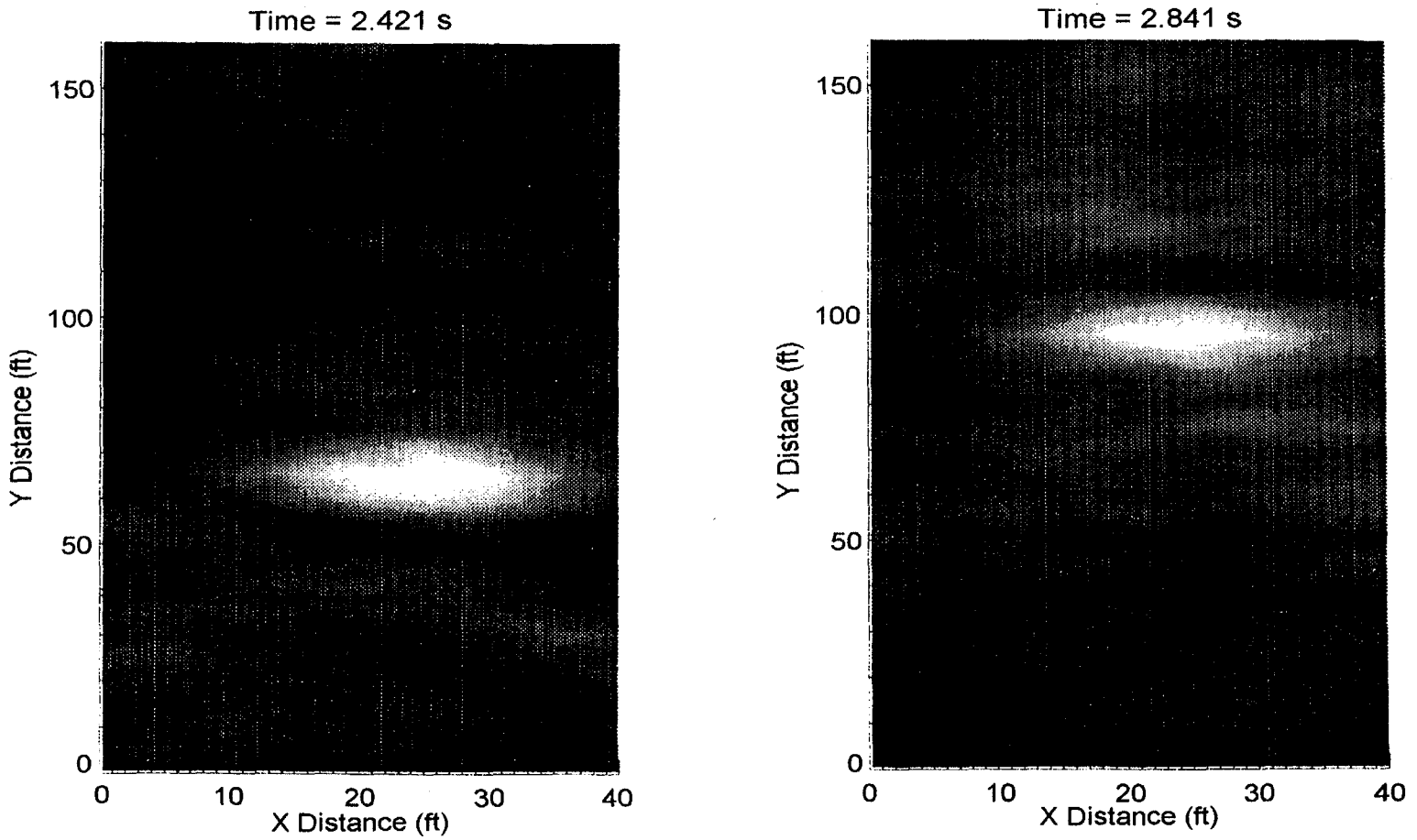

Figure 8: Plan view of road showing amplitude map of energy content of traces at two specific time slices. Axis represent x and y values of possible source locations. Bright spots show the source location with the greatest probability of being the source of the seismic energy, i.e. the vehicle location.

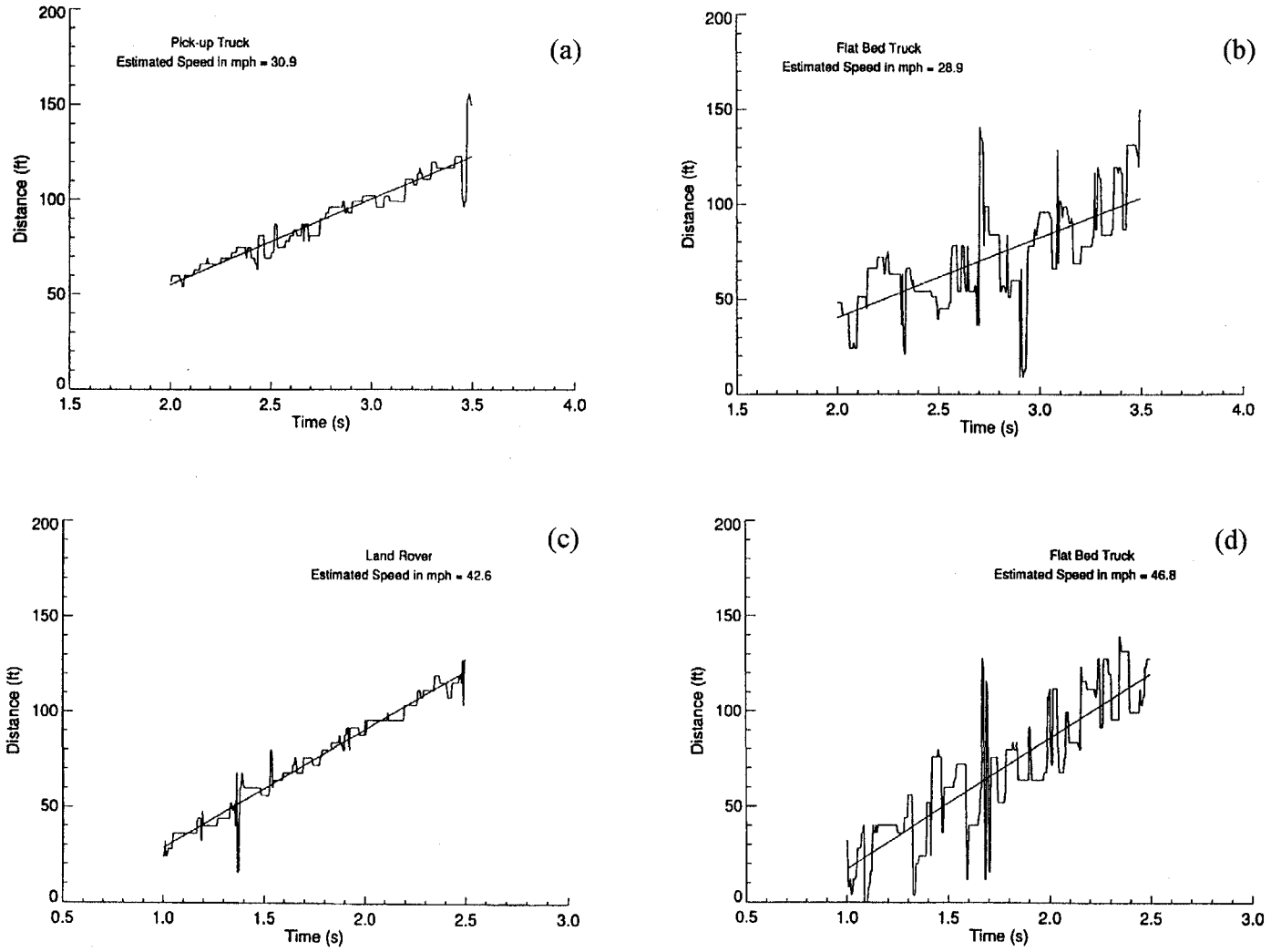

Figure 9: Plot of position of vehicle determined from amplitude map as a function of time. Straight lines are best fit to the data and are used to determine the stated velocities. Scatter in lines is related to wheel base length.

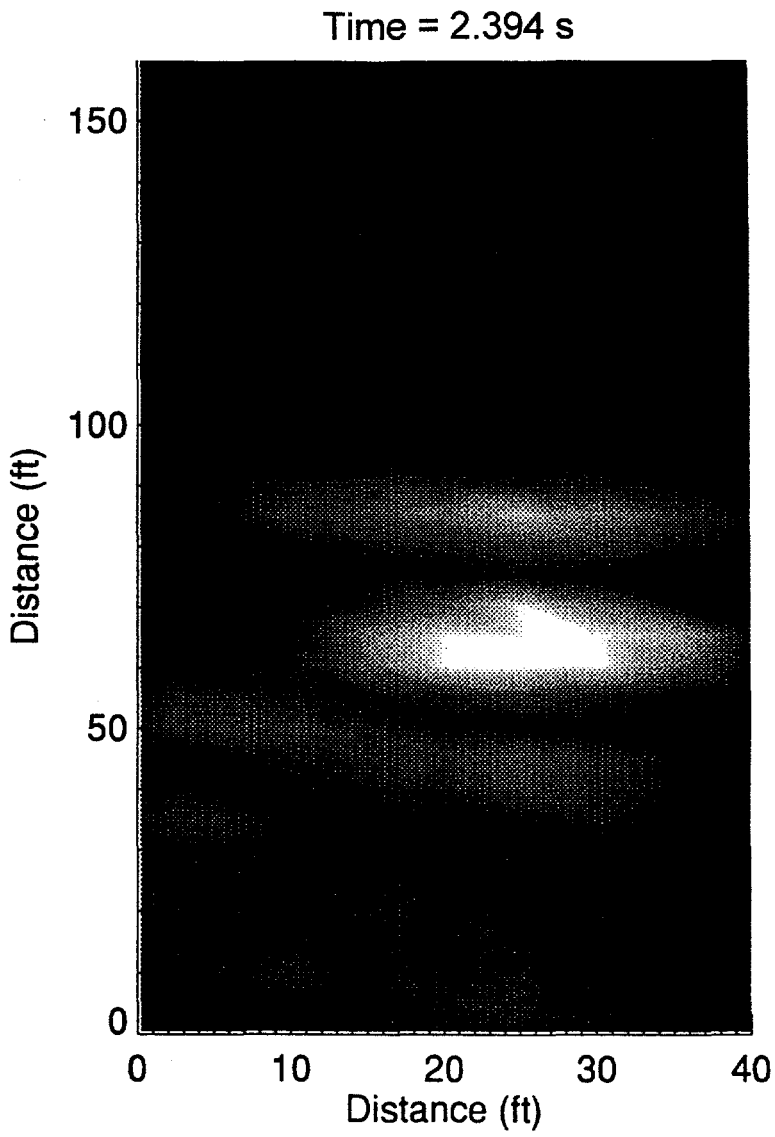

Figure 10: Amplitude map demonstrating splitting of the peak. This indicates energy being generated from the front and rear tires of the vehicle.

Vehicle	Wheel Base	Speed	Standard Deviation
Land Rover	7.3 ft.	43 mph	5.1 ft.
Pick-up Truck	12 ft.	31 mph	6.5 ft.
Utility Truck	13 ft.	31 mph	10.0 ft.
Utility Truck	13 ft.	53 mph	6.6 ft.
Flat-Bed Truck	no data	29 mph	20.2 ft.
Flat-Bed Truck	no data	47 mph	18.3 ft

Table 4: Comparison of wheel base length with standard deviation in vehicle position

Vehicle weight is another characteristic that should be expressed in the seismic signal, specifically in the amplitude of the signal. Figure 11 shows a comparison of vehicles at 30 mph (11a) and 50 mph (11b). A general correlation between weight and signal amplitude can be seen with amplitude increasing with weight. The exception to this trend is the flat-bed truck and the instrument truck in Figure 11a. Even though there is a significant increase in weight, the amplitudes of the signals are very similar, and the flat-bed signature is much more spread out in time.

To get a better understanding of the relationship between weight and amplitude, an estimate of the total energy of each trace for each vehicle was estimated by summing the time-window RMS amplitudes derived during the data normalization discussed in the section on the analysis of the passive seismic array. This gives single values for each trace which are plotted in Figure 12 for each vehicle at the speeds tested. The data are incomplete due to the loss of some traces resulting from equipment malfunctions. The similarity in the shape of the traces from vehicle to vehicle indicates that the location of the generation of the small seismic events is road dependent and not vehicle dependent.

Figure 12 again shows a general increase in amplitude with weight, except for the anomalous flat-bed data. Vehicle velocity appears to be a secondary minor effect, though this is partially due to the use of the same time window for both the 30-mph and 50-mph speeds. Since the AGC scaling values are calculated only for these time windows, a slower-moving vehicle will distribute the energy over more time windows compared to a faster moving vehicle, resulting in an apparent greater energy content. Similarly, a longer vehicle, such as the flat-bed truck, results in a longer signal length as can be seen in Figure 12b, and this may account for some of the apparent greater energy output for the flat bed compared to the instrument truck.

By examining the data from a specific sensor for all the vehicles, it may be possible to determine a trend in the weight versus amplitude relationship. Such a plot from the analysis of several sensors is shown in Figure 13. Except for the flat-bed data, the amplitude appears to increase monotonically with weight. However, further analyses with better control over vehicle weights and dimensions needs to be done before a believable relationship between weight and amplitude can be derived.

Analysis of Rincon Field Site Data

Passive Experiment

The data collected at the Rincon site had a much different character than that collected at the KAFB site. Figures 14 and 15 show data sections for a utility pickup truck and a double semi-truck respectively collected during the December (Figure 14) and March (Figure 15) surveys that can be compared to the section shown in Figure 6. Each of these figures shows a photograph of the vehicle passing through the array, the true amplitude data set, and the amplitude normalized data set. Unlike the data collected at KAFB, background noise at the Rincon site was significantly higher due to the type of generator used and nearby construction work. Several second-order, zero-phase Butterworth filters were applied to the raw data to produce the true amplitude sections shown in Figures 14b and 15b. To produce Figure 14b, a 510 Hz low-pass filter and notch filters between 4.5 - 9.0 Hz, 11 - 15 Hz, 55 - 60 Hz, and 100 - 120 Hz were applied. For Figure 15b, noise levels were greater, especially in the higher frequencies requiring a 250 Hz low-pass filter and notch filters at 60 - 75 Hz, 120 - 140 Hz, and 185 - 205 Hz to be applied.

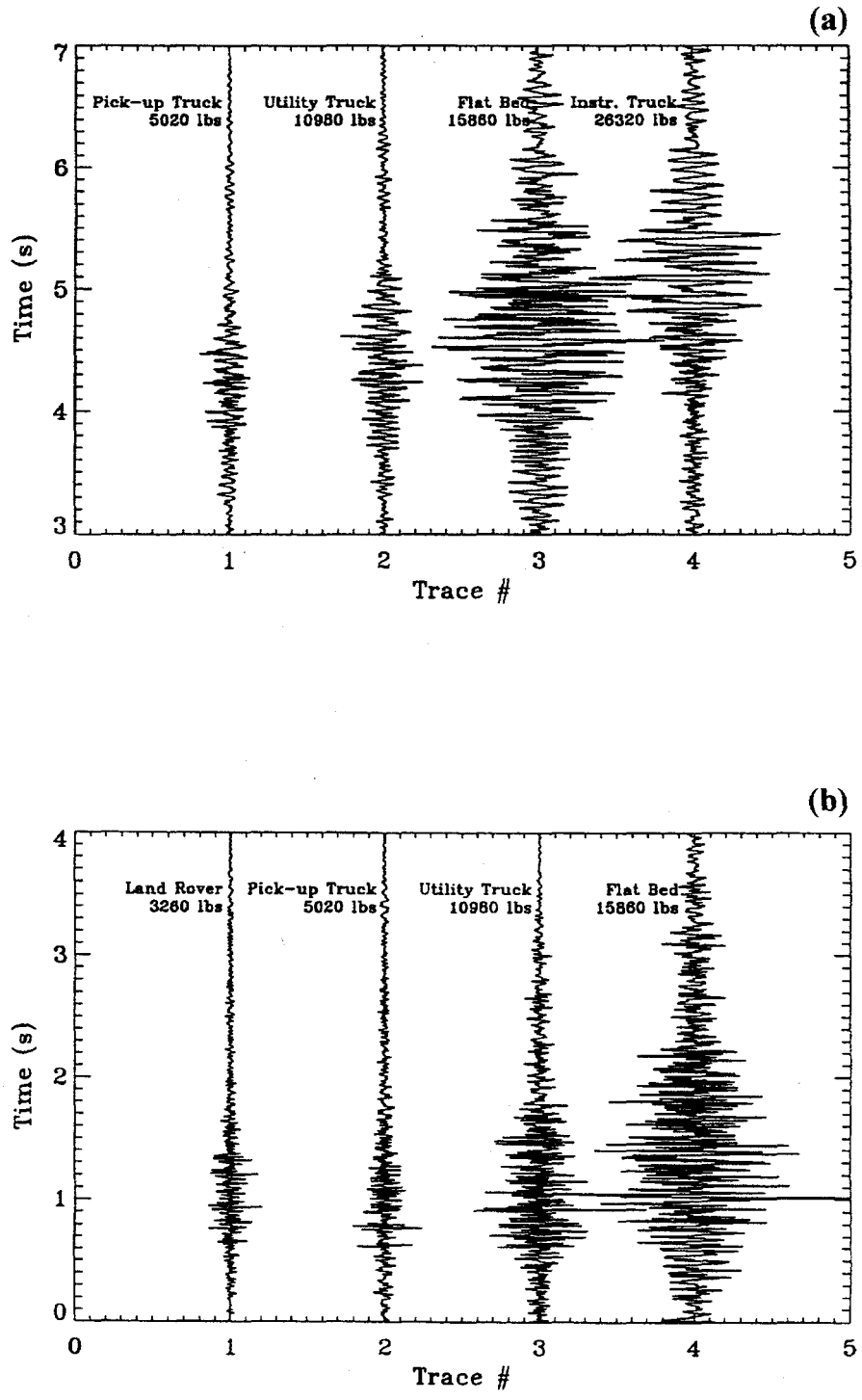

Figure 11: Comparison of wave amplitudes generated by different weight vehicles at 30 mph (a) and 50 mph(b).

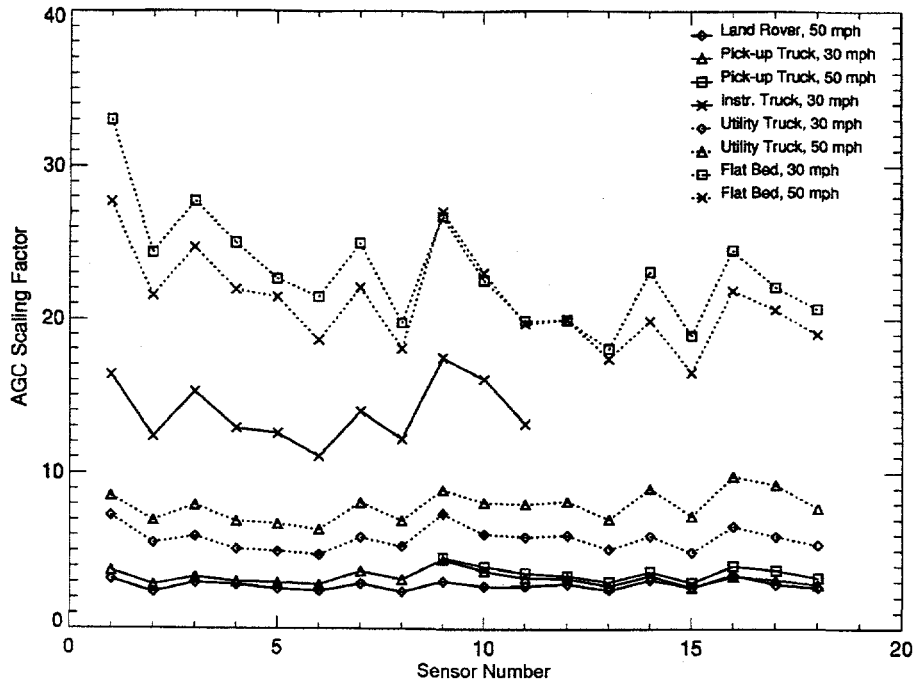

Figure 12: Comparison of overall signal amplitude for various vehicles, speeds, and sensors.

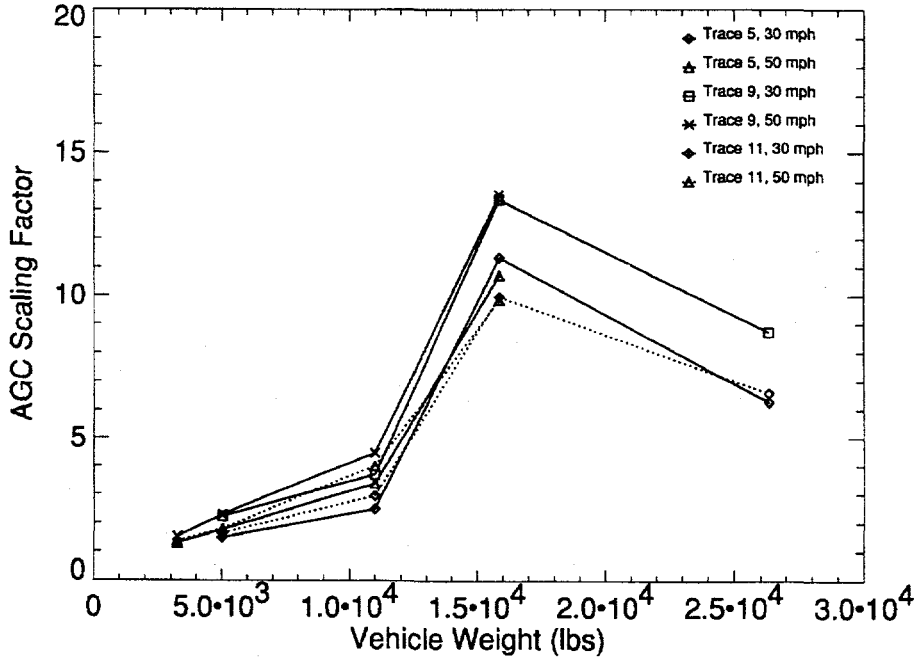

Figure 13: Comparison of overall trace amplitude as a function of vehicle weight for several stations.

For the Rincon vehicle monitoring, the general character of the wave packets is similar to the KAFB data, but there is a noticeable increase in frequency content and lack of the small seismic events traveling at the surface wave velocity noted in the KAFB data set. This is not to say that the small events are absent, but they are widely spaced with a low signal-to-noise ratio. Unfortunately, the full analysis of the data requires these events and, therefore, cannot be done on the Rincon data set. Some information can still be gleaned from these signals, though. A line fit through the center of the wavelet packets will still give a reasonable estimate of the vehicle velocity, as can be seen in the figures, and the amplitudes of the waves should contain information about the weight of the vehicle, as discussed in the previous section. These data were collected from vehicles in normal traffic, so no measure of true velocity or weight was available.

The lack of small seismic events itself provides information about the road surface. In the KAFB data, these events were controlled by the road surface and not the type or speed of the vehicle. The lack of events at Rincon suggests that the road has not worn enough to have flaws capable of generating the desired events. Continual monitoring of the road through such a passive array may pinpoint areas where pavement degradation is beginning by determining the source location of the small seismic events when they begin to appear.

During the second fielding at the Rincon site, we attempted to simulate flaws in the road by stringing cables across the road at regular intervals within the geophone array. It was hoped that vehicles striking these cables would create the desired small seismic events. Figure 16 shows an example for a small tank truck with the same filtering applied in Figure 16b as for Figure 15b. The presence of the cables did not result in any significant seismic events, probably due to the lack of good coupling between the cable and the road, but did produce a sharper spike in each of the wave packets that makes fitting a velocity line through the signal more precise.

The capability of the system to resolve multiple vehicles has not been thoroughly tested, but some data from multiple vehicles were collected for qualitative examination (Figure 17). In this example, the lead car is just exiting the array between sensors 6 and 7 at the initiation of recording. The last vehicle enters the array late in the recording widow ($\approx$ 2.6 s) with signal appearing on trace 1 and 12 first. The other two vehicles, traveling nearly side by side through the array, create the primary signal seen on the section. On first glance, it appears as though this signal is created by just one vehicle. On closer inspection, however, it is noted that the amplitude of the signal is about the same for sensors located on both sides of the road. In the single-vehicle sections studied before, the amplitudes were greater at the sensors closest to the lane in which the vehicle was traveling. If the amplitudes from both sides of the road are the same, the vehicle must be traveling down the center of the road, or two vehicles, one in each lane, must be present.

Closer inspection of traces 6 and 7 is even more revealing. These sensors are directly across the road from each other, yet trace 6 has its highest amplitude near the end of the wave packet while trace 7 has its highest amplitude early in the wave packet. Indeed, traces from opposite sides of the road through the whole array show this same pattern. This indicates that the lead vehicle (early high amplitudes) must be in the lane closest to sensors 7-12, i.e. the median lane, while the following vehicle must be in the shoulder lane. Inspection of the photograph in Figure 17a shows that this is indeed the case. These qualitative results bode well for the resolution of the method when multiple vehicles are present.

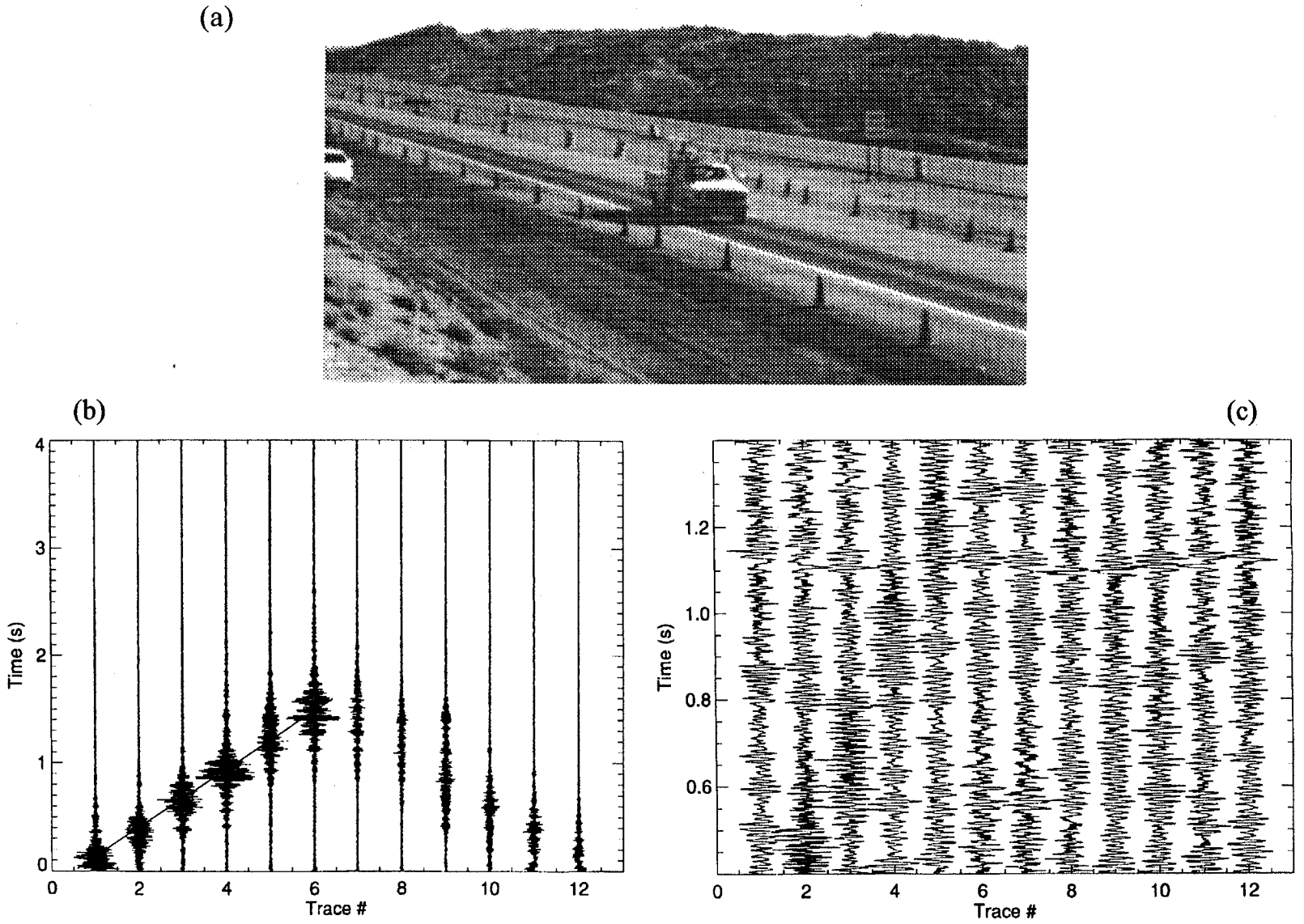

Figure 14: Example of passive data recorded during the first fielding at the Rincon test site. Estimated velocity of utility truck determined by graphically fit line is 70.5 mph

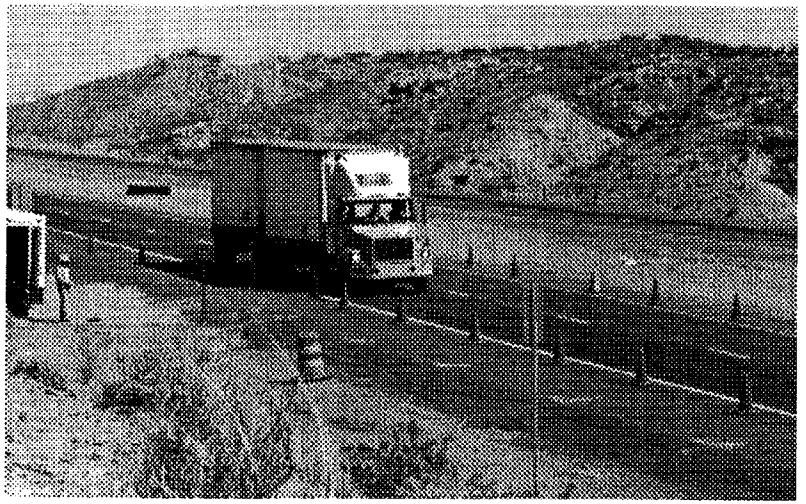

(a)

(b)

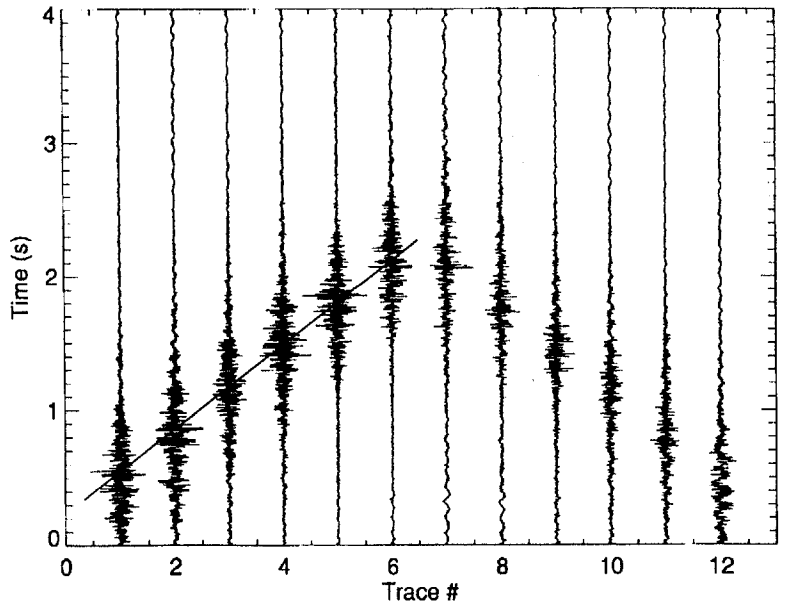

(c)

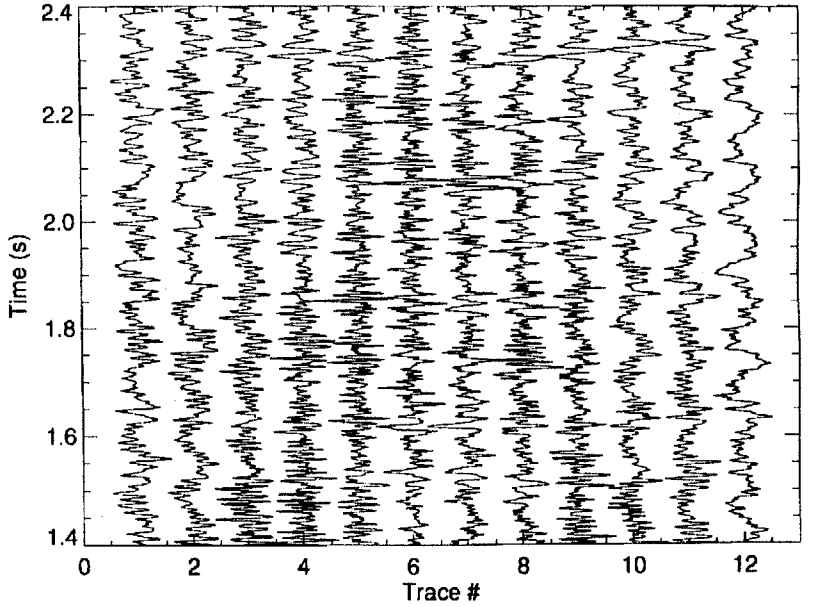

Figure 15: Example of data taken during second fielding at the Rincon site for double semi-truck. Estimated velocity of truck determined by graphically fit line is 65.4 mph.

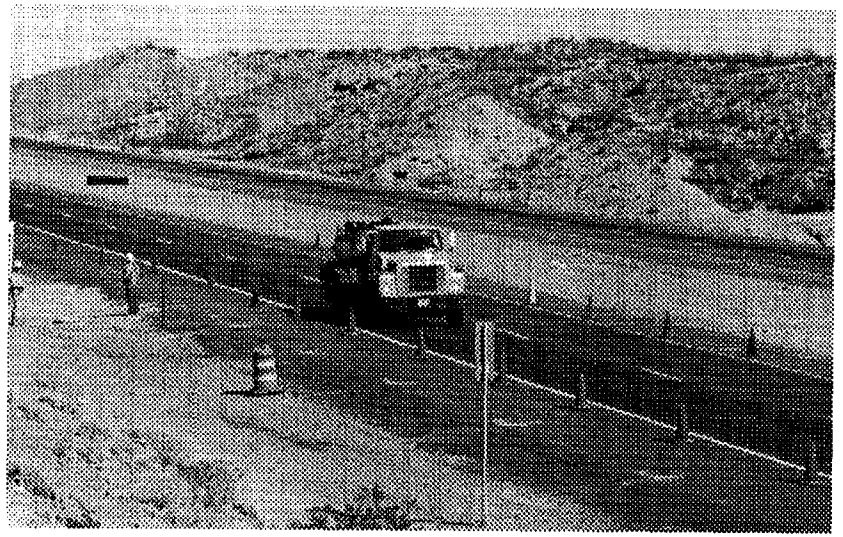

(a)

(b)

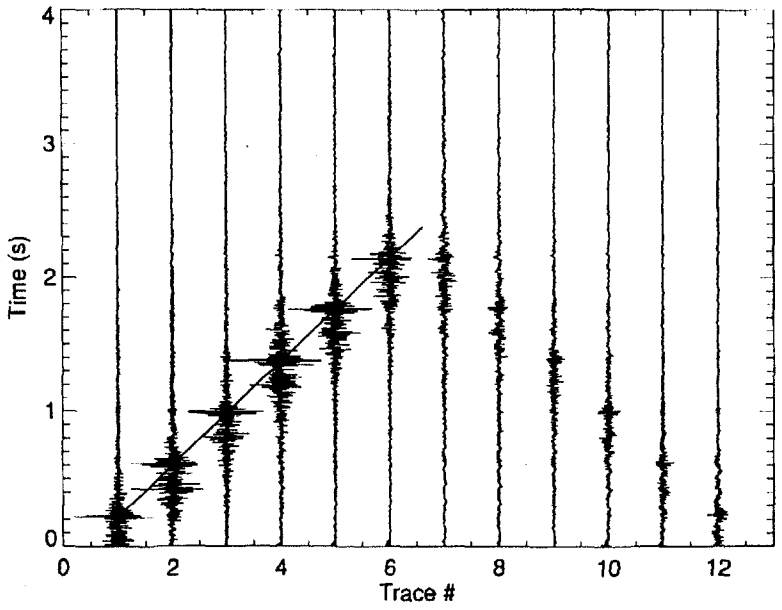

(c)

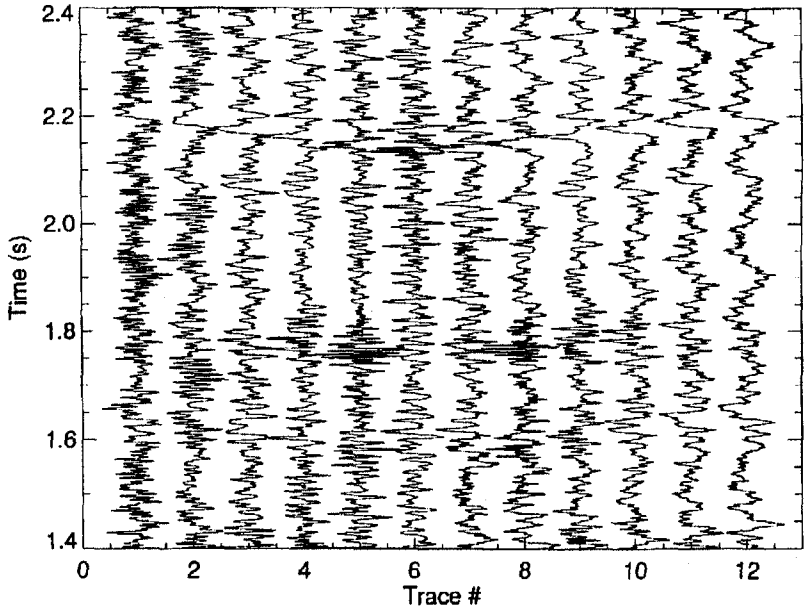

Figure 16: Example of data taken during second fielding at the Rincon test site with cables stretched across the road. Estimated velocity of small tank truck determined by graphically fit line is 53.3 mph.

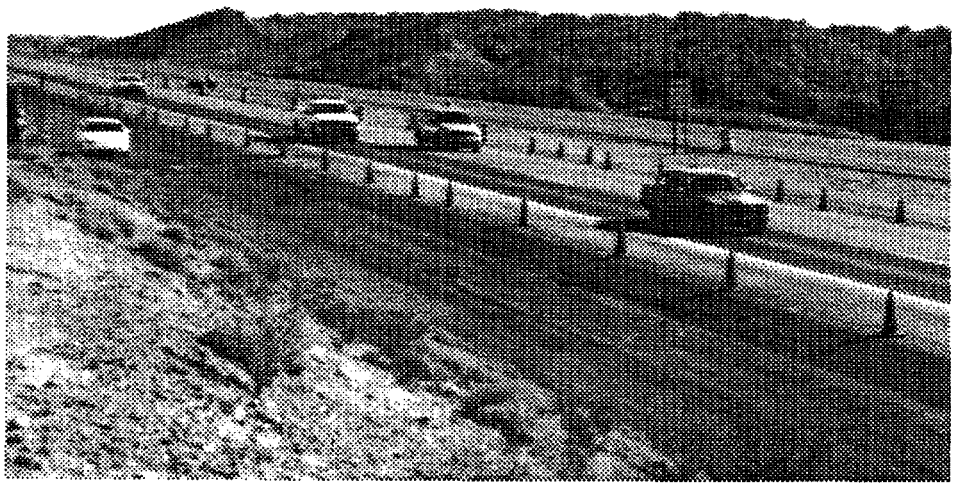

(a)

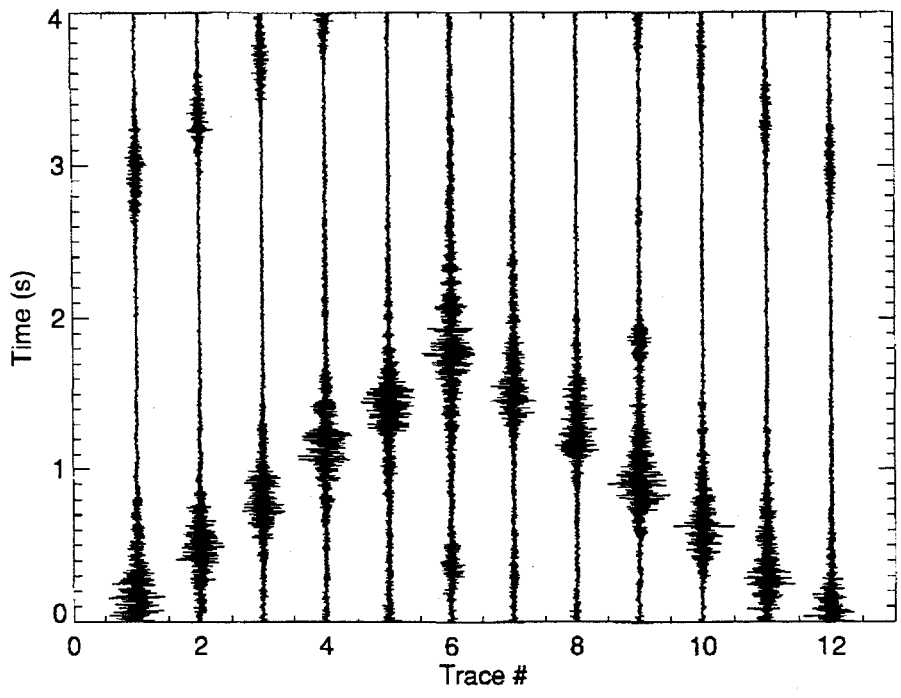

Figure 17: Example of data with multiple vehicles present in array.

Active Experiment

The primary focus of the active experiment is to determine the shear velocity structure of the pavement layering through the analysis of the surface wave dispersion, similar to the Spectral-Analysis-of-Surface-Waves (SASW) method of Nazarian et al. (1993). In general, surface or Rayleigh waves travel along the free surface of the earth with a retrograde elliptical particle motion. The surface wave is composed of a wide range of frequencies with a corresponding range of wavelengths. At lower frequencies, the seismic wavelengths are longer and penetrate to greater depths, encountering different seismic velocities under most circumstances. As a result, different frequencies of the surface waves will travel at different velocities, leading to dispersion of the total surface wave energy packet. By analyzing the dispersion of these surface waves, a one-dimensional shear-wave velocity structure of the near-surface can be determined.

The surface wave dispersion curves (plots of velocity as a function of wavelength) can be generated from plane-layered velocity models using the method of Haskell (1953). This method has been widely described in the literature (Schwab and Knopoff, 1970; Schwab and Knopoff, 1972; Takeuchi and Sato, 1972; Aki and Richards, 1980) and the reader is referred to these sources for additional details. More recently, variations of this method have been successfully applied to roadbed investigations by several authors (Hossain and Drenvich, 1989; Nazarian and Desai, 1993; Yuan and Nazarian, 1993). Our method attempts to build on these techniques by extending the area of the mapping by increasing the source-to-receiver separation while still maintaining high enough frequencies to resolve the details in the pavement structure.

For our tests, we attempted to directly measure the velocity of the surface waves by narrow band-pass filtering of a broadband source (sledge hammer), and by direct generation of narrow-band waves with short monofrequency bursts generated by the magnetostrictive vibrator.

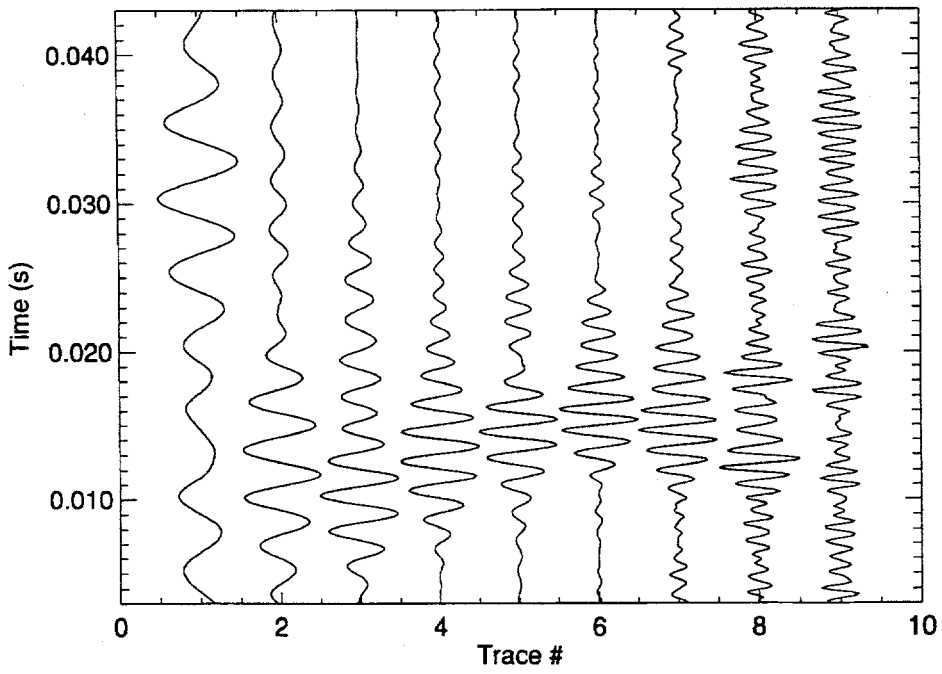

Figure 18: Processed data from monofrequency bursts during first Rincon fielding with source at station 1 and receiver directly across the road at station 12. Traces used bursts 100 Hz apart in frequency so that trace 1 was generated with a 200 Hz burst and trace 9 with a 1000 Hz burst.

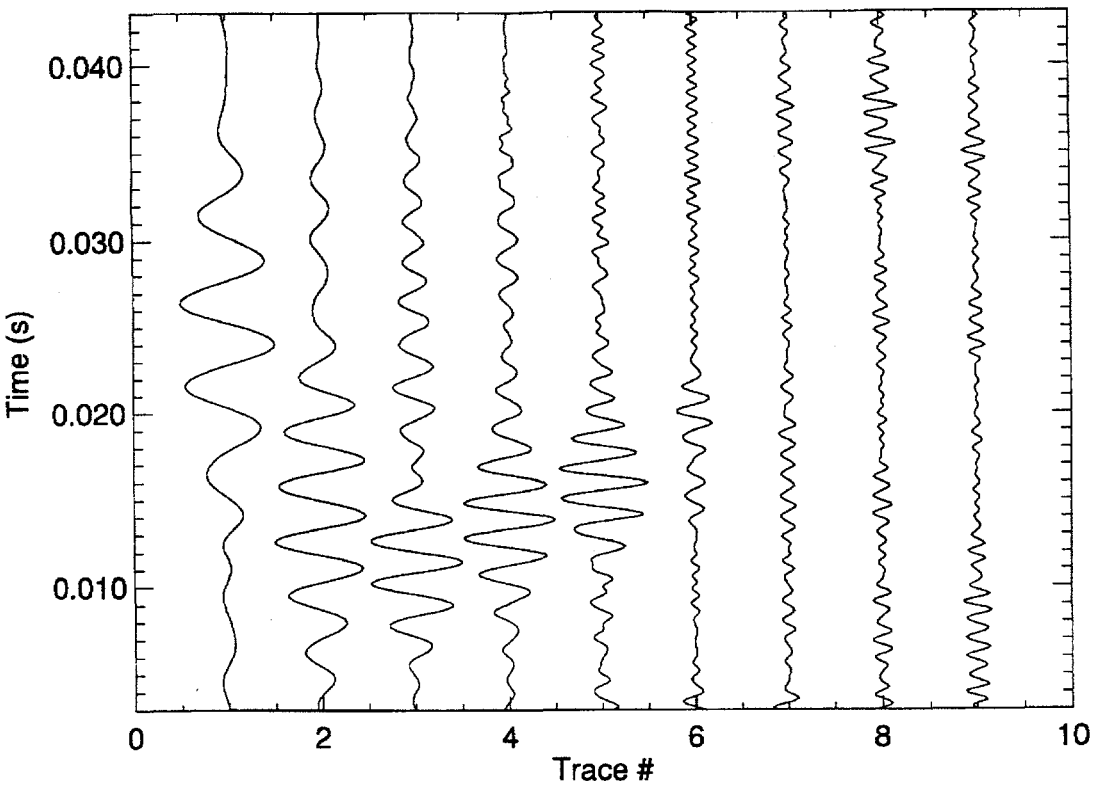

Figure 19: Processed data from monofrequency bursts during second Rincon fielding with source at station 1 and receiver directly across the road at station 12. Traces used burst 100 Hz apart in frequency so that trace 1 was generated with a 200 Hz burst and trace 9 with a 1000 Hz burst.

The monofrequency bursts from the vibrator yielded the most promising results. To enhance the surface wave arrivals, processed data were created by crosscorrelating the recorded data with the source signature. Crosscorrelation is a mathematical process that compares the source signature with the recorded signal and amplifies those parts of the signal most similar to the source signature. The processed traces for the first Rincon fielding, where the mounting plates were bolted directly to the pavement, are shown in Figure 18. The processed records show a wavelet packet at the time of arrival. There is some ambiguity as to which arrival this packet represents: the compressional, shear, or surface wave. In most cases, the surface wave is the highest amplitude arrival and for this reason, the surface wave arrival time is picked at the center of the wavelet as indicated. There is a good possibility that this arrival is contaminated with body wave arrivals that may lead to timing errors. Some of this ambiguity might be resolved by examining the polarization of the wavelets, but this was not pursued under the present study. With the time picks chosen, travel times can be calculated for frequencies up to 700 Hz.

When the mounting plates were bolted onto the concrete plugs that were epoxied into the pavement, the range of useable frequencies was extended to 800 Hz (Figure 19). This indicates that the second method of coupling both the source and the receivers is much more efficient, especially for the higher frequencies. The question still remains, however, as to whether the frequencies generated will have the resolution necessary to provide information on the pavement structure.

To test this, three different velocity models representing possible velocity structures for the pavement at the site were created (Figure 20). The models consisted of three pavement layers representing the PMBP layer, the bituminous treated base, and the Type IB base all underlain by a constant-velocity halfspace. In Models 1 and 2, this halfspace had the same shear-wave velocity of 3450 ft/s, whereas in Model 3 it was slightly higher at 3600 ft/s. Models 1 and 2 were also similar in the pavement portion of the velocity structure, with velocities decreasing with depth.

Model 1 had a slightly higher surface layer velocity with slightly lower basal layer velocities. Model 3 was significantly different with a low-velocity middle layer between two higher velocity layers.

Dispersion curves were generated for each of these three models (Figure 21). The curves are essentially identical at wavelengths greater than 1 m, with most of the variation occurring at wavelengths less than 0.7 m. Unfortunately, even the best of the Rincon data sets had a minimum analyzable wavelength of 0.9 m. From this we can conclude that under the conditions at the Rincon site, it is not possible to resolve changes in the pavement with the present method. This is primarily due to the loss of the high frequency energy through attenuation and inefficient coupling.

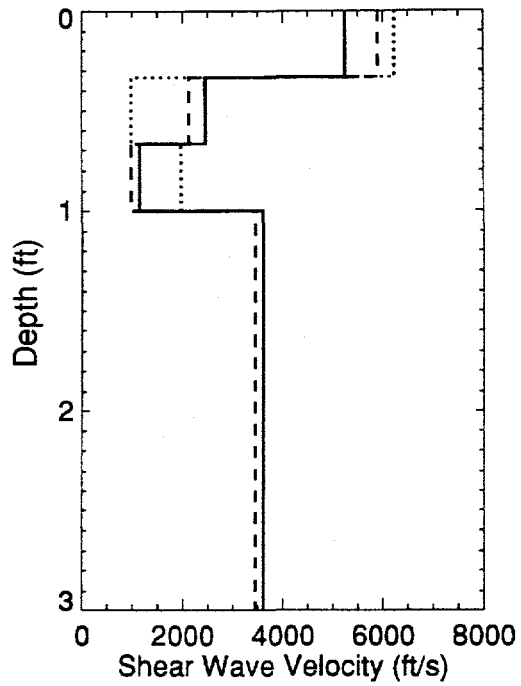

Figure 20: Shear-wave velocity models used for testing sensitivity of surface wave dispersion analysis. Model 1 displayed as dotted line, Model 2 as dashed, and Model 3 as solid.

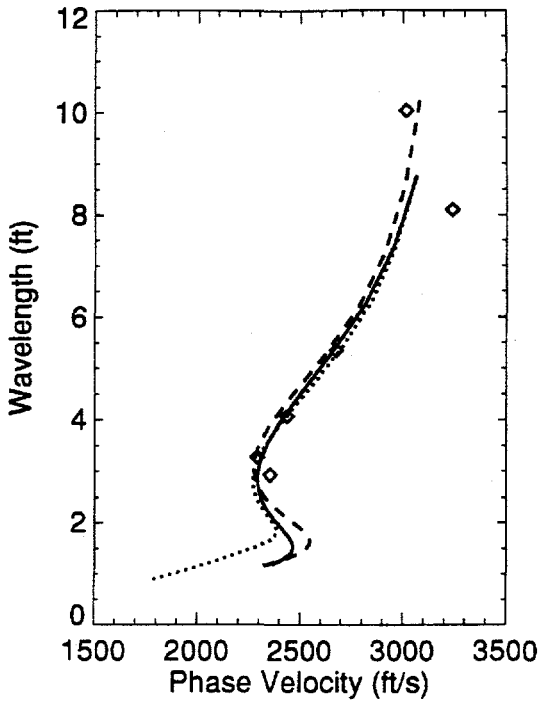

Figure 21: Surface wave dispersion curves generated from velocity models in Figure 20. Line styles (solid, dashed, or dotted) in this figure correspond to the velocity models with the same line style in Figure 20. Diamonds indicate data points taken from Figure 19.

FUTURE DIRECTIONS

These preliminary studies and analyses have pointed out a number of areas where further work needs to be done. In the active portion of the experiment, the lack of high frequencies in the received signal and the ambiguity of the identification of the arrival made good modeling impossible. Closer spacing between the sources and receivers would significantly improve the resolution by preserving the higher frequency energy. Likewise, increasing the power output of the source, especially at the higher frequencies, may make this a feasible technique, although a different coupling mechanism would be required. Embedding the sources within the pavement with epoxy or cement may be a feasible way of ensuring good coupling. Examination of the polarization of the recorded signals may aid in arrival identification, and examination of the wavelet phase may provide better timing of the surface wave arrival.

Results from the passive portion of the experiment were very promising, but there are still several areas where ambiguities need to be resolved. Of particular interest is getting a better determination of the relationship between signal amplitude and vehicle weight. This can only be obtained by a better understanding of the source mechanism of the seismic events coupled with better controlled field studies. The field studies should be designed to isolate the effect of weight on signal amplitude by varying the weight of a single vehicle and measuring the amplitude change. They should also examine the other characteristics that may affect amplitude by

measuring the signal from vehicles of varying length and number of axles but equal weights, and by measuring signals from the same vehicle traveling at a variety of speeds.

Model studies to ascertain the exact source mechanism of the seismic energy will enable us to understand exactly which vehicle and road features have the greatest effect on the signal generated. In addition, this will allow the creation of synthetic data to test a great number of possible vehicle sizes, weights, and combinations without a massive field effort.

Finally, improvements need to be made in fielding methods, including better methods for coupling sensors and sources to the pavement, more reliable recording equipment, and determination of the optimal sensor type for both the active and passive experiments.

CONCLUSIONS

Data from the active experiments examining pavement characteristics did not produce favorable results in this experiment due to the poor coupling of the required high frequency energy. There is potential for determining pavement velocity structure and characteristics from this method, but a significant amount of research is still needed to refine this method.

Results from the passive studies were much more promising and have shown that there is a great amount of information about the vehicle contained in the seismic signal. It has been demonstrated that the seismic signal can be recorded and analyzed to determine both the vehicle location at any point in time and the vehicle velocity. Rough estimates of vehicle size and weight can also be extracted from the seismic signal, but further work on refining these methods is needed. The results obtained at any site are a function of the pavement surface affecting the capabilities of the analysis method and also opening up the possibility of using passive monitoring of vehicles to obtain information about the pavement itself.

REFERENCES

Aki, K. And Richards, P.G (1980). *Quantitative Seismology: Theory and Methods*, Vol. 1, W. H. Freeman and Co., San Fransisco.

Haskell, N. A. (1953). "The dispersion of surface waves in multilayered media" *Bulletin of the Seismological Society of America*, Vol. 43, 17-34.

Hossain, M. M. and Drenvich, V. P. (1989). " Numerical and optimization techniques applied to surface waves for backcalculation of layer moduli." *Nondestructive pavements and backcalculation of layer moduli; ASTM STP 1026,* A. J. Bush III and G. Y. Baladi, eds. ASTM, Philadelphia, 649-669.

Nazarian, S. and Desai, M. R. (1993). "Automated surface wave method: Field testing." *Journal of Geotechnical Engineering,* Vol. 119, No. 7, 1094-1111.

Nazarian, S., Baker, M. R., and Crain, K. (1993). *Developing and Testing of a Seismic Pavement Analyzer*, Strategic Highway Research Program Report # Contract H-104B, Strategic Highway Research Program, National Research Council, Washington, D.C.

Schwab, F., and Knopoff, L. (1970). "Surface wave dispersion computations." *Bulletin of the Seismological Society of America*, Vol. 60, 321-344.

Schwab, F., and Knopoff, L. (1972). "Fast surface wave and free mode computations." *In* B. A. Bolt (editor), *Seismology: Surface waves and Earth Oscillations (*Methods in Computational Physics, Vol. 11), Academic Press, New York., 82-152.

Takeuchi, S., and Sato, T. (1972). "Seismic surface waves." *In* B. A. Bolt (editor), *Seismology: Surface waves and Earth Oscillations (*Methods in Computational Physics, Vol. 11), Academic Press, New York, 201-223.

Yuan, D., and Nazarian, S. (1993). "Automated surface wave method: Inversion technique." *Journal of Geotechnical Engineering,* Vol. 119, No. 7, 1112-1126.

DISTRIBUTION

10 W. L. Barringer, P. E.
Research Engineer
New Mexico State Highway and Transportation Department
1001 University Blvd. SE, Suite 103
Albuquerque, NM 87106

1 Alan C. Chachich
Massachusetts Institute of Technology
Center for Transportation Studies
3 Cambridge Center, Rm. 208
Cambridge, MA 02142

1 Gordon McKeen, P. E.
New Mexico Engineering Research Institute
University of New Mexico
1001 University Blvd. SE
Suite 103
Albuquerque, NM 87106

1 Soheil Nazarian
University of Texas at El Paso
Department of Civil Engineering
El Paso, TX 79968-0516

1 Karen Wenzel
Southern California Association of Governments
818 West Seventh Street, 12th Floor
Los Angeles, CA 90017-3435

5	0537	Richard C. Ormesher, 2344
1	0750	Laurence S. Costin, 6117
20	0750	Gregory J. Elbring, 6116
5	0750	David J. Holcomb, 6117
1	0750	Marianne C. Walck, 6116
1	0860	Bernard J. Gomez, 2522
1	0877	Daniel H. Cress, 5933
1	0985	Donald H. Schroeder, 2605
1	9018	Central Technical Files, 8940-2
5	0899	Technical Library, 4916
2	0619	Review & Approval Desk, 12690 For DOE/OSTI